AGU PUBLICATIONS

JGR

Journal of Geophysical Research: Space Physics

RESEARCH ARTICLE
10.1002/2017JA024445

Simulated Prompt Acceleration of Multi-MeV Electrons by the 17 March 2015 Interplanetary Shock

Mary Hudson[1], Allison Jaynes[2], Brian Kress[3], Zhao Li[1], Maulik Patel[1], Xiao-Chen Shen[4,5], Scott Thaller[6], Michael Wiltberger[5], and John Wygant[6]

[1]Department of Physics and Astronomy, Dartmouth College, Hanover, NH, USA, [2]Laboratory for Atmospheric and Space Physics, University of Colorado Boulder, Boulder, CO, USA, [3]Cooperative Institute for Research in Environmental Sciences, University of Colorado Boulder, Boulder, CO, USA, [4]Shandong Provincial Key Laboratory of Optical Astronomy and Solar-Terrestrial Environment, Institute of Space Sciences, Shandong University, Weihai, China, [5]High Altitude Observatory, National Center for Atmospheric Research, Boulder, CO, USA, [6]School of Physics and Astronomy, University of Minnesota, Twin Cities, Minneapolis, MN, USA

Abstract Prompt enhancement of relativistic electron flux at $L = 3–5$ has been reported from Van Allen Probes Relativistic Electron Proton Telescope (REPT) measurements associated with the 17 March 2015 interplanetary shock compression of the dayside magnetosphere. Acceleration by ~1 MeV is inferred on less than a drift timescale as seen in prior shock compression events, which launch a magnetosonic azimuthal electric field impulse tailward. This impulse propagates from the dayside around the flanks accelerating electrons in drift resonance at the dusk flank. Such longitudinally localized acceleration events produce a drift echo signature which was seen at > 1 MeV energy on both Van Allen Probe spacecraft, with sustained observations by Probe B outbound at $L = 5$ at 2100 MLT at the time of impulse arrival, measured by the Electric Fields and Waves instrument. MHD test particle simulations are presented which reproduce drift echo features observed in the REPT measurements at Probe B, including the energy and pitch angle dependence of drift echoes observed. While the flux enhancement was short lived for this event due to subsequent inward motion of the magnetopause, stronger events with larger electric field impulses, as observed in March 1991 and the Halloween 2003 storm, produce enhancements which can be quantified by the inward radial transport and energization determined by the induction electric field resulting from dayside compression.

Key Points:
- Prompt MeV electron enhancement at $L = 3–5$ is seen in Van Allen Probes measurements from 17 March 2015 IP shock magnetopause compression
- MHD test particle simulations reproduce drift echoes observed by the REPT instrument
- Azimuthal electric field impulse responsible for acceleration and radial transport is consistent with EFW measurements

Correspondence to:
M. Hudson,
Mary.K.Hudson@Dartmouth.edu

Citation:
Hudson, M., Jaynes, A., Kress, B. T., Li, Z., Patel, M., Shen, X.-C., … Wygant, J. (2017). Simulated prompt acceleration of multi-MeV electrons by the 17 March 2015 interplanetary shock. *Journal of Geophysical Research: Space Physics*, *122*, 10,036–10,046. https://doi.org/10.1002/2017JA024445

Received 14 JUN 2017
Accepted 15 SEP 2017
Accepted article online 20 SEP 2017
Published online 14 OCT 2017

1. Introduction

Prompt acceleration of radiation belt electrons by an interplanetary shock compression of the dayside magnetopause was first reported for the 24 March 1991 geomagnetic storm observed by the Combined Release and Radiation Effects Satellite (CRRES), which was launched into a geosynchronous transfer orbit (GTO) on 25 July 1990 and lasted 14 months on orbit (Blake et al., 1992). CRRES was located on the nightside at 2200 MLT for this event and observed both the compressional B_z component of the magnetic field and azimuthal E_Φ component of the electric field, which is the signature of a magnetosonic impulse launched within the magnetosphere by a sudden dayside magnetopause compression (Li et al., 1993; Wygant et al., 1994). Most remarkably, the energetic particle instruments on CRRES recorded an increase in flux of ~ 15 MeV electrons as well as multi-MeV protons with a peaked spectrum and recurrent drift echoes consistent with injection into $L \sim 2.5\ R_E$, the usual flux-depleted slot region (Lyons et al., 1972), on a drift timescale. Recurrent drift echoes were observed (Blake et al., 1992), explained by injection occurring over a localized range of longitude along the dusk (dawn) flank for electrons (protons) as electrons (protons) drifted synchronously with the magnetosonic impulse spreading toward the nightside. While the first simple model prescribed the magnetosonic impulse electric field responsible for electron acceleration and inward radial transport and energization conserving the first invariant (Gannon et al., 2005; Hudson et al., 1995; Li et al., 1993), subsequent MHD simulations reproduced the peaked spectrum and radial location of the new electron (Elkington et al., 2004) and proton (Hudson et al., 1997) belts, with assumed solar wind parameters in the absence of upstream observations at the time of CRRES. A similar shock injection event was observed for the 2003 Halloween storm (Looper et al., 2005) and simulated with measured upstream solar wind parameters but absent the in situ

particles and fields measurements in the near equatorial plane available from CRRES (Kress et al., 2007). The acceleration mechanism was illuminated by these global MHD simulations, which has become the standard for modeling such events (Hudson et al., 2015).

The twin Van Allen Probes spacecraft were launched on 30 August 2012 (Mauk et al., 2013) into a slightly lower apogee transfer orbit than CRRES (5.8 R_E × 600 km) with solar wind measurements available continuously at L1 and auxiliary measurements available from other spacecraft such as Geotail (Nishida, 1994) and Acceleration, Reconnection, Turbulence and Electrodynamics of the Moon's Interaction with the Sun (ARTEMIS) (Angelopoulos, 2011), the latter a pair from the Time History of Events and Macroscale Interactions during Substorms (THEMIS) mission now in lunar orbit. The Energetic Particle, Composition, and Thermal Plasma (ECT) suite (Spence et al., 2013) and the Electric Fields and Waves (EFW) instruments on Van Allen Probes (Wygant et al., 2013) provide much higher time resolution than previously available as well as spatial separation between identical spacecraft in approximately the same orbit (slightly different apogee produces variable separation), which can be useful for timing measurements of the magnetosonic impulse propagation speed and energetic electron drift echoes, flux, energy, and pitch angle modification following interplanetary shock compression. Two recent events have been analyzed for their similarity to the March 1991 event in effect on multi-MeV electrons: though less extreme, the 7 October 2013 and 17 March 2015 interplanetary (IP) shock compressions of the dayside magnetopause produced multi-MeV electron enhancements on less than a drift timescale (Baker et al., 2016; Foster et al., 2015; Kanekal et al., 2016). Drift echoes are also seen from substorm injection events at lower ~ 100 keV energies (Claudepierre et al., 2013), where the azimuthal electric field associated with substorm dipolarization plays a similar role as that due to dayside magnetopause compression (Li et al., 1998). This paper focuses on the latter, specifically modeling the 17 March 2015 event, since the 7 October 2013 injection has been studied previously (Foster et al., 2015; Hudson et al., 2015). What we present here beyond prior MHD test particle modeling is a simulation of the drift echoes detected by a virtual satellite in the computational domain along with pitch angle distributions which show evidence for drift shell splitting and magnetopause loss. These simulation results are compared directly with the ECT observations.

In section 2 the modeling tools are described. Section 3 presents observations from the ECT and EFW instruments on Van Allen Probes for the 17 March 2015 IP shock arrival interval and results from corresponding MHD and test particle simulations. Section 4 analyzes the acceleration implied by the simulated azimuthal electric field with conclusions presented in section 5.

2. Model

A set of modeling tools has been developed to examine the global dynamics of electrons in the magnetosphere using measured upstream solar wind parameters as the outer boundary condition on solution of the ideal MHD equations. The Lyon-Fedder-Mobarry code is used with a computational domain which extends from +30 R_E to −300 R_E along SM-x and from −150 R_E to +150 R_E along SM-y and SM-z (Lyon et al., 2004). All MHD input variables are assumed to be uniform in y-z at the upstream boundary. MHD input parameters for the 17 March 2015 storm were taken from OMNIWeb, plotted for the 2 day storm interval in Li et al. (2017) (Figure 1). The irregular grid with resolution 106 × 96 × 128 along radial, azimuthal, and polar directions includes a higher density of grid points in regions of stronger gradients, so for example, the Earth's bow shock and magnetopause. The inner boundary is taken to be a sphere at 2 R_E geocentric radius, with coupling to the ionosphere using an electrostatic potential solver which incorporates dynamic changes in field-aligned currents and modified conductivities (Merkin & Lyon, 2010). The Rice Convection Model has been coupled to Lyon-Fedder-Mobarry (LFM) to include ring current drift physics (Pembroke et al., 2012). The MHD fields were dumped at a 1 s cadence to resolve the rapid change in electric field amplitude (e.g., 5 mV/m in 30 s) as seen by multi-MeV drifting electrons. A key additional tool for radiation belt modeling is the "rbelt3d" code developed at Dartmouth (Kress et al., 2007), which advances Lorentz and guiding center electron (or proton) trajectories in 3-D using a switch based on the level of first adiabatic invariant conservation (Kress et al., 2007), following trajectories as test particles in the output fields from the LFM simulations, weighting to particle flux with an assumed spectral model (Kress et al., 2007). Simulated electron flux is weighted in energy and L using the European Space Agency radiation belt electron flux model from CRRES satellite measurements (Vampola, 1996) in previous studies (Kress et al., 2007, 2014). Here we perform the flux weighting using ECT measurements from the orbit prior to shock arrival. With these tools we can follow test particle dynamics including

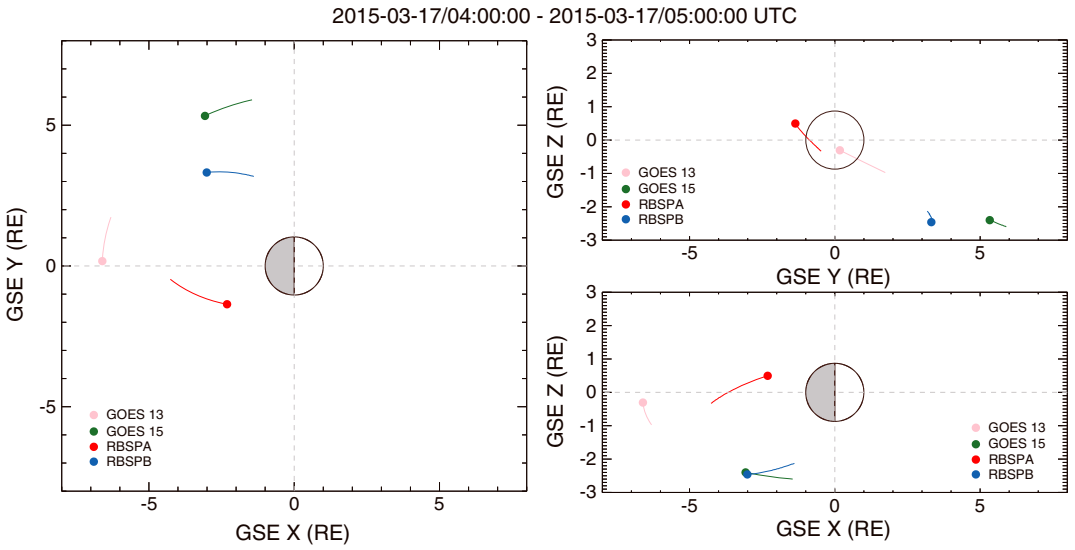

Figure 1. Location of the Van Allen Probes and GOES 13 and 15 spacecraft at the time of the interplanetary shock arrival on 17 March 2015 ~ 0445 UT at the magnetopause (Kanekal et al., 2016).

response to ultralow frequency (ULF) waves that cause inward radial transport and energization for an outward radial gradient as well as enhanced loss to the magnetopause for inward gradient (Elkington et al., 2003; Shprits et al., 2006) and the response to impulsive electric fields as modeled here.

3. Observations and Simulation Results

Figure 1 shows the location of the Van Allen Probes and GOES 13 and 15 spacecraft at the time of the interplanetary shock arrival at the magnetopause for a 1 h interval centered on 17 March 2015 at ~ 0445 UT. Figure 2 extends Figure 7b from the Baker et al. (2016) measurements by the Relativistic Electron Proton Telescope component of the ECT instrument suite on Van Allen Probe B at $L = 5$ at the time of the IP shock arrival at Earth. Four energy channels are plotted versus time showing (1) drift echoes with decreasing period as energy increases from 1.8 to 3.4 MeV and (2) a minimum flux at 90° pitch angle (arrow), which broadens in pitch angle as the spacecraft moves outward in L. This minimum is absent at lower L values and emerges as the spacecraft moves outward. A dropout in flux centered on 90° pitch angle is the first indication of the IP shock arrival prior to the first drift echo. Note by contrast that the flux peaked at 90° in measurements from Probe A at $L = 3$ at the time of IP shock arrival, as reported by Kanekal et al. (2016) and Baker et al. (2016), where drift shell splitting (Hudson et al., 2012; Sibeck et al., 1987) and magnetopause shadowing are expected to have negligible effect, also evident in the low L value portion of Figure 2, left.

Figure 3 shows measurements of the three GSM components of the electric field impulse by the EFW instrument on Probe B at the time of impulse arrival ~ 0447 UT. The measured E field was converted from "modified GSE" coordinates, which assume that mGSE-x is along the nearly sun-aligned spin axis of the spacecraft (Wygant et al., 2013), into GSM coordinates. The assumption that $E_x = 0$ in mGSE coordinates is made, since the E_x component cannot be obtained reliably from $\mathbf{E} \cdot \mathbf{B} = 0$. The $\mathbf{E} \cdot \mathbf{B} = 0$ assumption fails for conversion of the two-component spin plane measurements to a vector measurement when B is within ~ 20° of the spin plane (Ali et al., 2016), as is the case during the time interval plotted. The magnitude of the dominant y component, which is positive when E_Φ is negative, is comparable in magnitude to the value of E_Φ determined from the MHD simulations (Figure 4) at the location of Probe B. Simulated E_Φ will be used to calculate the acceleration of electrons producing the observed drift echoes, since the global E_Φ distribution is required along the electron drift trajectory.

Figure 4 shows the azimuthal electric field impulse from the LFM-RCM (LFM coupled to Rice Convection Model) simulations at the azimuthal and radial location of Probe B, which was outbound at $L = 5$ and 21 MLT at ~ 0447 UT when the impulse arrived. Simulated fields and corresponding effects on electrons are shifted in run time to coincide with the observed arrival time of the electric field impulse at Probe B plotted in Figure 3. This corrects for the assumption of uniform solar wind input parameters at $x = 30\ R_E$, propagated from

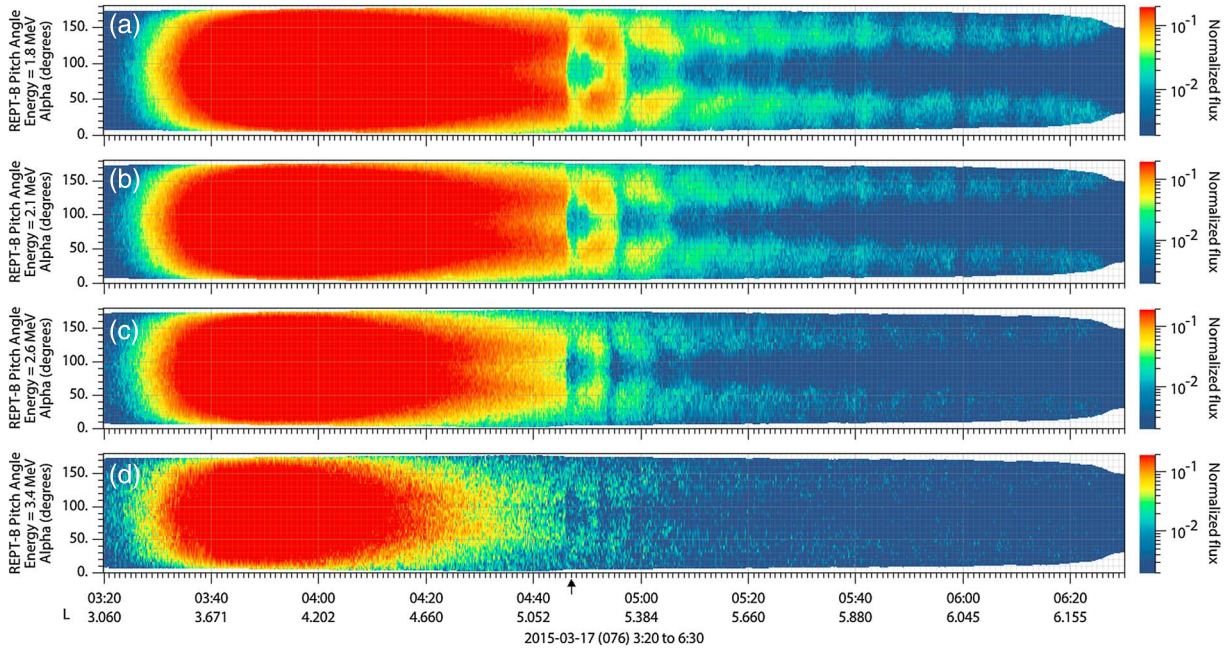

Figure 2. Pitch angle distribution plots of (a) 1.8, (b) 2.1, (c) 2.6, and (d) 3.4 MeV electrons, where color indicates particle intensity measured at Van Allen Probe B for the period 0320 to 0630 UT which encompasses the arrival of the IP shock at ~ 0445 UT at the magnetopause. Probe B is outbound at $L \sim 5$ at 0447 and detects a minimum in flux at 90° prior to the shock arrival which broadens in pitch angle as the spacecraft moves outward toward the magnetopause. Drift echoes are evident with decreasing period as energy increases. Arrow indicates E_Φ impulse arrival at Probe B.

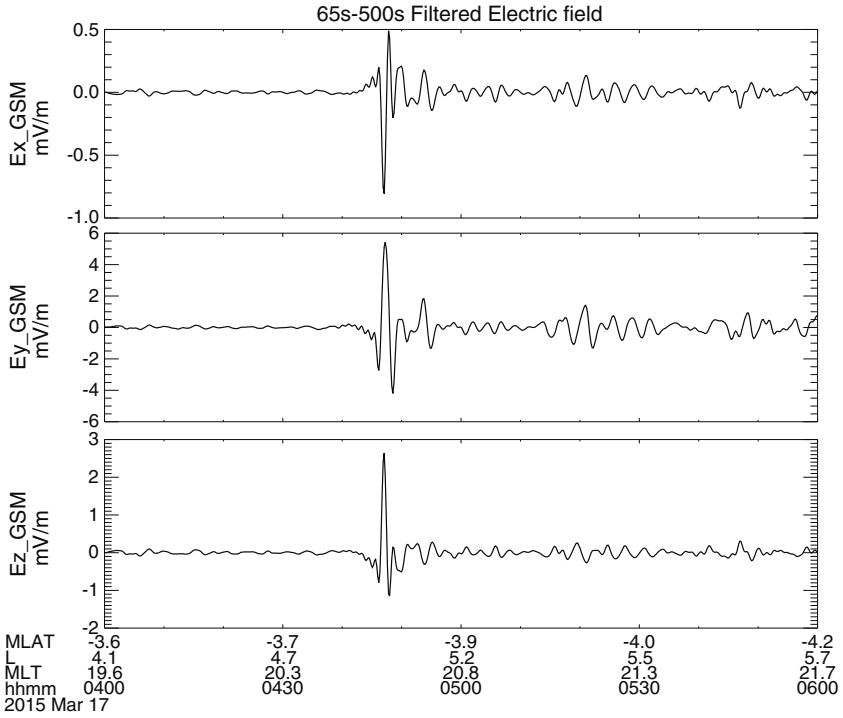

Figure 3. Measurements of the three GSM components of the electric field impulse by the EFW instrument on Probe B at the time of impulse arrival ~ 0447 UT.

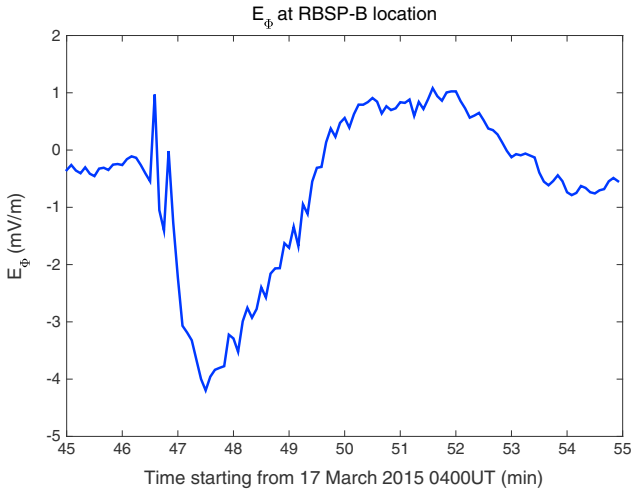

Figure 4. Azimuthal electric field impulse E_Φ in the equatorial plane from the LFM simulations at the azimuthal and radial location of Probe B, which was outbound at $L = 5$, MLT = 2030 at ~ 0447 UT when the impulse arrived.

L1 measurements, such that arrival time and location of the CME shock along the magnetopause will not be exact. Probe A was inbound postmidnight near $L = 3$ when the IP shock hit the magnetosphere and moved inside the "impenetrable barrier" to multi-MeV electrons (Baker et al., 2014, 2016). Thus, measurements from Probe B are more useful for examining the impulsive acceleration process.

Figure 5 shows snapshots of the azimuthal electric field in the equatorial plane from the MHD simulation prior to and during the impulse arrival at Probe B. It is this field which produces acceleration and inward radial transport conserving the first invariant, with largest effect on electrons of comparable drift velocity to the impulse propagation speed (Elkington et al., 2002). A magnetosonic impulse also propagates around dawn in the direction of ion drift; however, there are no MeV ions with a comparable azimuthal drift velocity for this event, essential for the drift-resonant acceleration mechanism described below, in contrast to events with a significant solar energetic proton source population such as March 1991, produced by a very high speed IP shock and associated flare (Hudson et al., 1997).

Because the Van Allen Probe spacecraft were separated by $\Delta L \sim 2$ at the time of impulse arrival, it is more useful to use the GOES 13 and 15 geosynchronous spacecraft for this event to determine the azimuthal propagation speed of the magnetosonic impulse, which determines the energy of electrons most affected by E_Φ (Elkington et al., 2002). The impulse arrival time is 04:46:26 UT at GOES 15 and 04:47:08 UT at GOES 13, which gives a propagation speed of 1,048 km/s between the two spacecraft separated by 4 h of MLT. This is a reasonable magnetosonic speed, dominated by the Alfven speed in the outer magnetosphere (Paral et al., 2015). In the MHD simulation the delay time between the arrival of the magnetic field perturbation at the two GOES spacecraft yields 1,300 km/s, due to a lower plasma density simulated in the absence of ionospheric outflow.

Figure 6 shows the result of weighted test particle flux summed over pitch angle run through the MHD fields accumulated in a 0.5 R_E radius disc in the SM equatorial plane centered at Probe B moving outward in L at the time of the MHD impulse arrival when it was at $L = 5$ and 2100 MLT. Weighting is performed as a postprocessing step on an initially flat distribution of test particles in energy (1–7 MeV) and pitch angle (40°–140°). The weighting uses flux from the ECT instrument measured on the previous orbit; see Figure 6b. The resulting acceleration of multi-MeV electrons is observed along with drift echoes, which follow from coherent

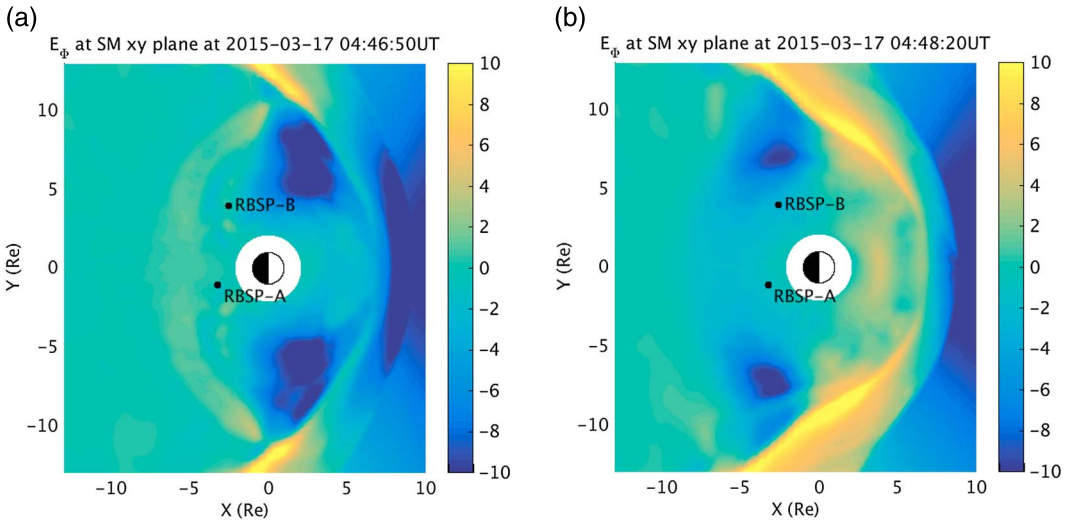

Figure 5. Snapshot of the azimuthal electric field in the equatorial plane from the MHD simulations (a) prior to and (b) during the impulse arrival at Probe B. Location of Probe A and B mapped to the equatorial plane is indicated.

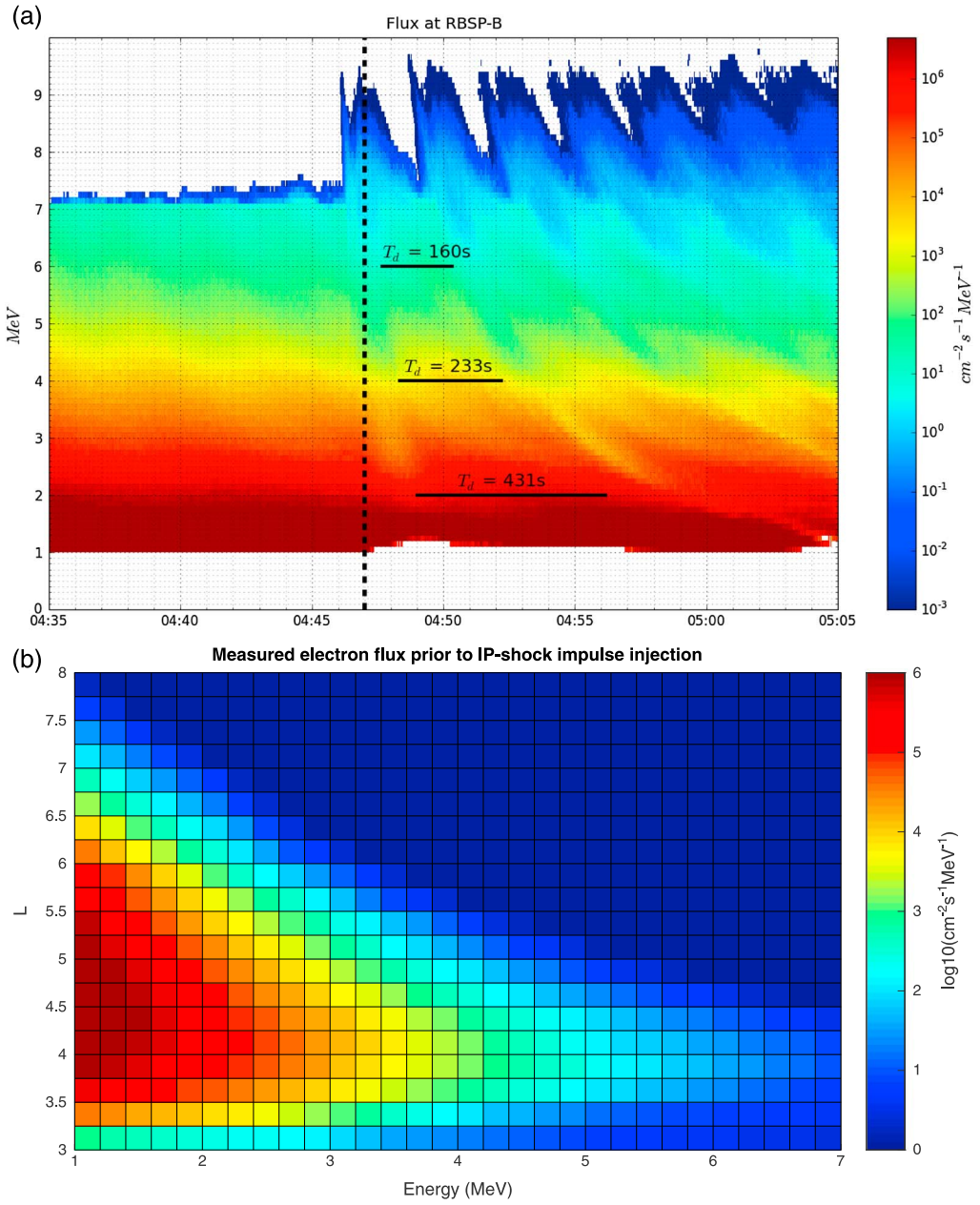

Figure 6. (a) Weighted test particle flux summed over pitch angle run for 5.1 M particles through the MHD fields accumulated in a 0.5 R_E radius disc in the SM equatorial plane centered on Probe B location as it moves outward in L from $L = 5$ at 2100 MLT at time of E_Φ impulse arrival. Dashed vertical line indicates impulse arrival at 0445 UT at the magnetopause. Test particles are initiated in the equatorial plane with a flat energy spectrum between 1 and 7 MeV, between $L = 3$ and 8, and flat pitch angles between 40° and 140° (Kress et al., 2007). Weighting is applied as a postprocessing step using (b) measured electron flux from ECT on Probe B for the orbit prior to IP shock impulse injection shown in Figure 6a ($L > 6$ and $E > 6.2$ region are extrapolated from measurement).

acceleration by the azimuthal electric field impulse in Figure 5, as it propagates from the dayside around to dusk and midnight in the direction of electron drift.

Figure 7 shows snapshots of a subset of electrons at 2–2.1 MeV, from the population used to produce Figure 6 at the location of Probe B. The background gray scale indicates negative E_Φ. Color indicates energy in MeV at the time plotted. Acceleration of electrons drifting with the negative E_Φ impulse along the dusk flank is evident.

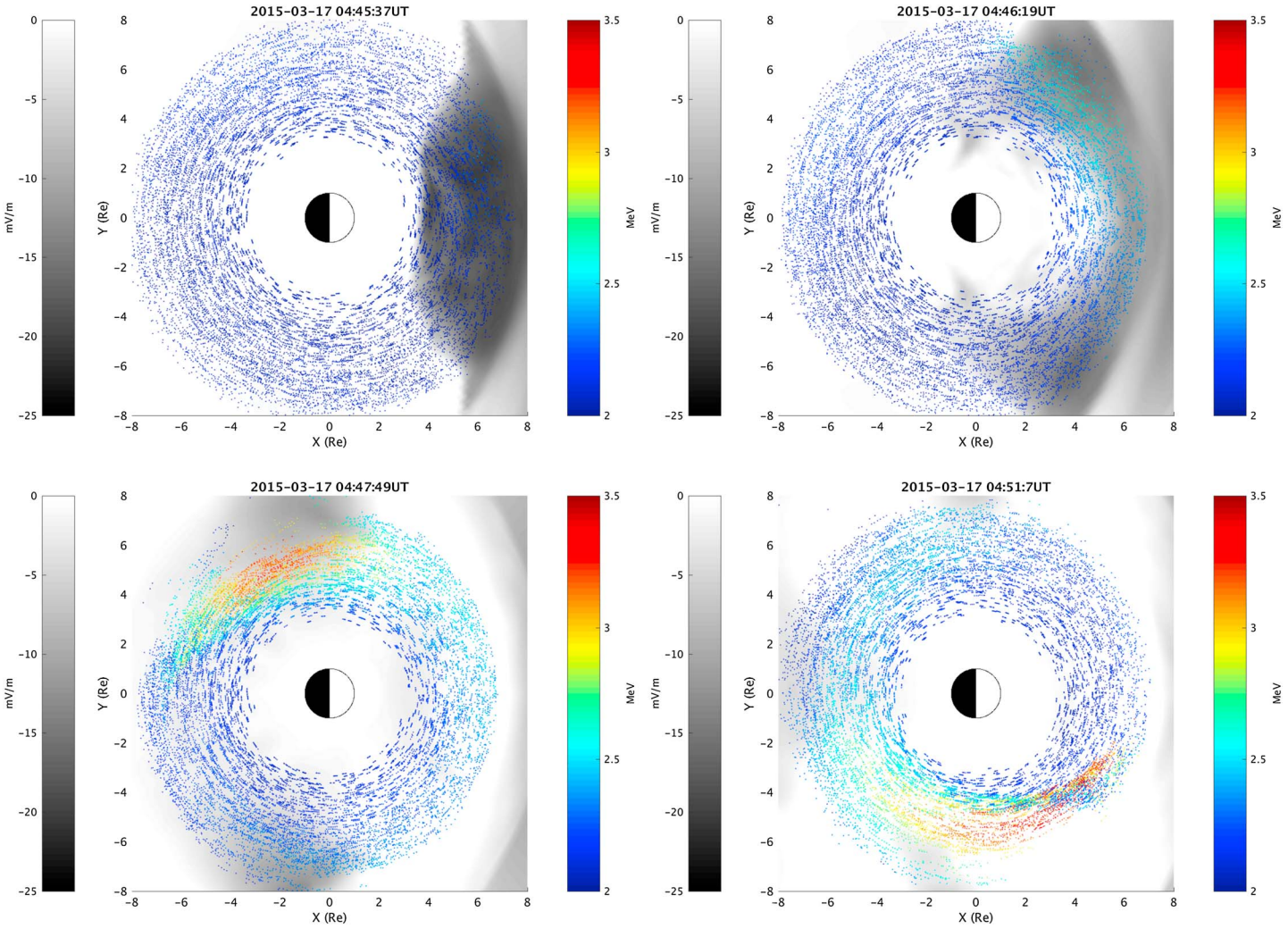

Figure 7. Snapshots of a subset of test particles with initial energy 2.0–2.1 MeV, with energy of test particles at time plotted indicated in color scale and E_Φ plotted in gray scale.

4. Discussion

A similar analysis to that of Foster et al. (2015) for the 7 October 2013 IP shock injection event, which produced multi-MeV electron drift echoes observed by both Van Allen Probes spacecraft on the dayside, will be followed for the 17 March 2015 event. Assume that an electron interacts with the impulse in Figure 5 as the impulse propagates and the electron drifts from noon to midnight around the dusk flank. An electron drifting at the same speed as the magnetosonic impulse will see an approximately constant electric field in its frame of reference and optimize the energy gain, while electrons drifting faster or slower will spend less time with the pulse. An electron with an azimuthal propagation speed of 1,048 km/s at $L = 6.6$ (observed from the impulse delay between GOES 13 and 15) has a drift period of 250 s at an energy of 2.6 MeV, consistent with the drift echo observations in Figure 2. The energy range for drift resonance spans the energy range of Figure 2 since the E_Φ impulse is broad, as seen in Figure 5 (Elkington et al., 2002). The azimuthal distance traversed at $L = 6.6$ is, for example, $\sim$ 132,000 km from noon to midnight and the electric field experienced at the maximum is $\sim$ 10 mV/m in Figure 5a, yielding an energy gain of $\sim$ 1.3 MeV if an electron experiences the full field strength over the assumed distance. The electron, however, moves inward in L conserving its first invariant, with final to initial energy scaling with final to initial L as $W_f/W_0 \sim (L_0/L_f)^{3/2}$ in the relativistic limit assuming a dipole

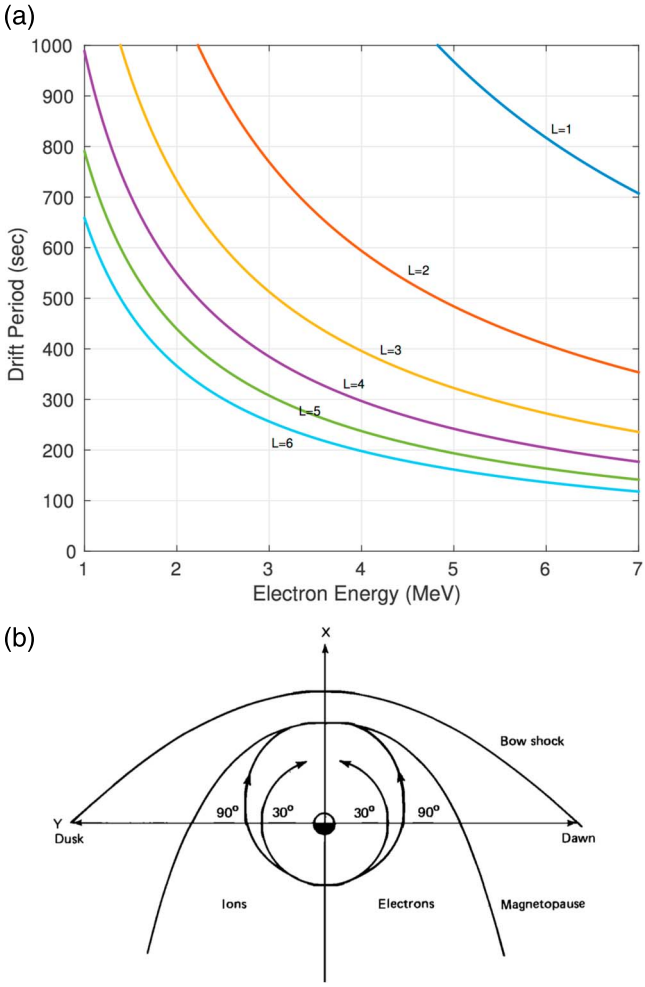

Figure 8. (a) Drift period versus electron energy at different L in a dipole. (b) Drift shell splitting of 90° electrons relative to 30° electrons in a compressed dipole drifting from night to dayside (Sibeck et al., 1987; Roederer, 1970).

magnetic field, where energy and momentum scale as $W \sim pc$, with p the perpendicular momentum and c the speed of light. As an example, a 1.7 MeV electron at $L = 6.6$ becomes a 2.8 MeV electron at $L = 5$, using the exact relativistic formula for energy including rest mass, for an energy gain of 1.1 MeV. This acceleration increases the flux at a given L in a fixed energy channel as measured by the REPT instrument. This mechanism only operates along the dusk flank to accelerate electrons since they are propagating opposite to the tailward drift of the impulse along the dawn flank (see Figure 5). Thus, drift phase bunching occurs due to acceleration over a limited range of longitude, assumed to be 180° here as in the estimate by Wygant et al. (1994) for the March 1991 injection event. Drift echoes are expected that correspond to the drift period in a dipole magnetic field, depending on electron energy and L: $T_d = 2\pi\gamma q L^2 R_E^2/3\mu$ for equatorially mirroring electrons (Schulz and Lanzerotti, 1974). Here γ is the Lorentz factor, q is charge, and $\mu \sim W_\perp/B$ in the weak relativistic limit becomes pc/B in the strongly relativistic limit, with B the local magnetic field strength.

Figure 8a plots drift period versus electron energy at different L values for 90° pitch angles in a dipole field, showing that a 2.1 MeV electron at $L = 5$ has a 7.3 min (438 s) drift period, consistent with the drift echo observations in Figure 2b. Examination of Figure 6 from the MHD test particle simulations shows the energy dependence of the resulting drift echoes with flux peaks more widely separated at lower energies and lines indicating the calculated dipole drift period at 2, 4, and 6 MeV at $L = 5$. Figure 8b sketches the drift orbits of 90° and 30° pitch angle electrons launched from the same equatorial plane location on the nightside in a compressed dipole, producing drift shell splitting (Sibeck et al., 1987; Roederer, 1970) with arrival at different radial locations on the dayside, top of figure. This affects pitch angle distributions described next.

Figure 9 plots simulated pitch angle distributions in four energy ranges overlapping with REPT measurements at 1.8, 2.1, 2.6, and 3.4 MeV. These plots show drift echo dependence on pitch angle, with flux minima at 90° for electrons drifting in synch along the dusk flank with the predominantly negative azimuthal electric field impulse, seen in Figure 4. Electrons at other longitudes not drifting in synch with E_Φ establish a 90° flux peak due to bounce loss. The flux minimum about 90° produced by E_Φ is consistent with drift shell splitting and loss to the magnetopause enhanced by inward motion of the magnetopause following IP shock compression (Hudson et al., 2014; Sibeck et al., 1987). Sibeck et al. (1987) showed that pitch angle dispersion due to drift shell splitting depends on the sign of the radial gradient. As shown schematically in Figure 8b, electrons launched on the nightside with 90° pitch angle drift outward on the dayside relative to those at 30° pitch angle, as the 90° electrons conserve only the first invariant, while 30° electrons must conserve both first and second. This phenomenon of drift shell splitting in a nondipolar field, compressed on the dayside and stretched on the nightside, results in decrease in 90° flux relative to 30° flux on a steep inward radial gradient as is seen at $L = 5$ in Figure 6b. This results in a lower flux at 90° at each instant of the drift echo enhancement. The opposite effect was seen on the inner gradient of the outer zone for the 7 October 2013 injection event; see Foster et al. (2015) Figure 4 for Van Allen Probe A. Their Figure 6 shows the drift echoes at 3.6 MeV and delay for Van Allen Probe A trailing Probe B, which sees the drift echoes on the outer gradient of the outer zone. The resulting minima at 90° are absent at lower L values, e.g., $L = 3.67$ in Figure 2, and become broader in pitch angle about 90° as the spacecraft moves outward in L as expected for drift shell splitting, since dipole distortion increases, both before shock arrival and subsequently in the drift echoes evident in Figure 2.

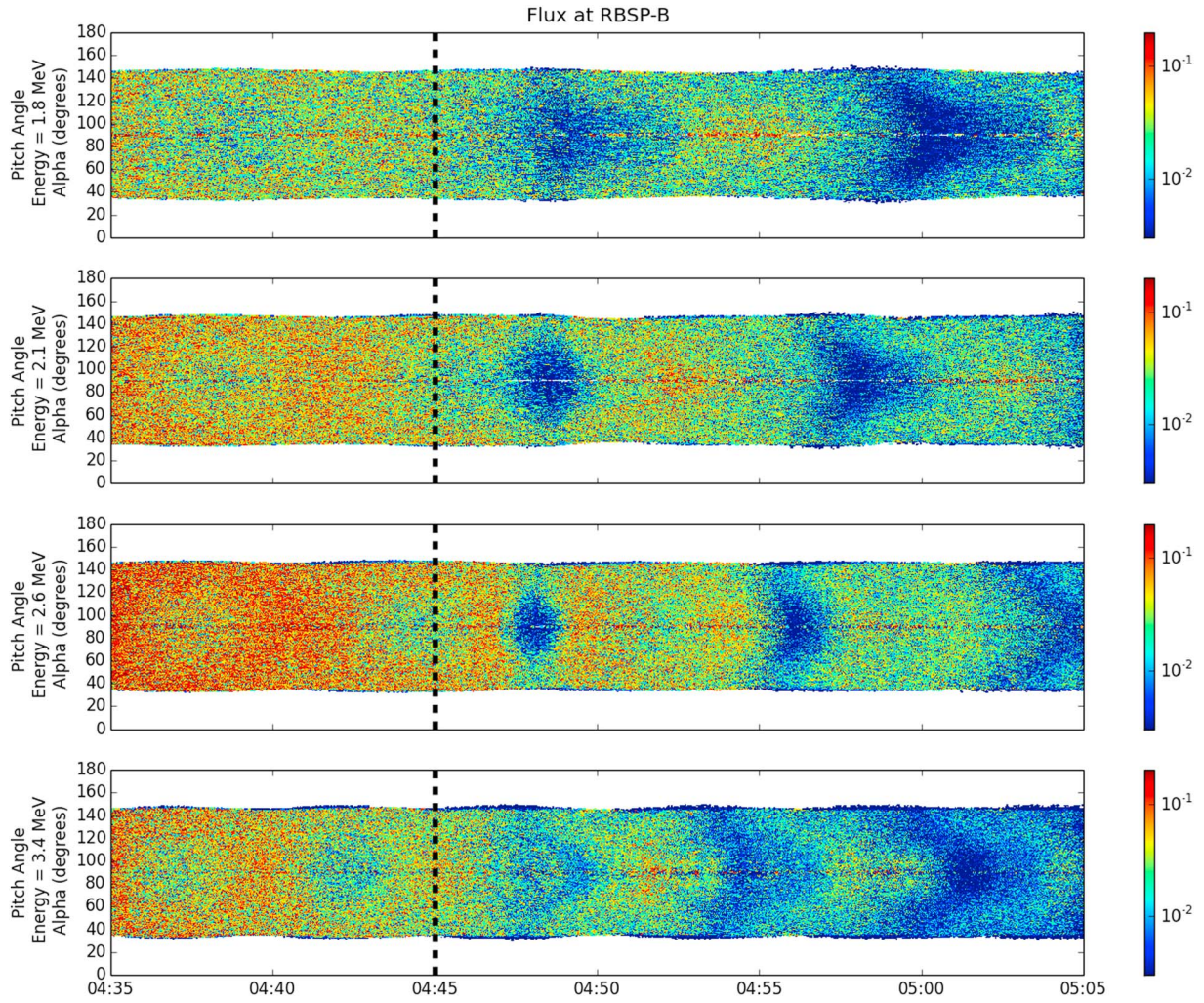

Figure 9. Simulated pitch angle distributions in normalized flux at 1.8 MeV, 2.1 MeV, 2.6 MeV, and 3.4 MeV, which show drift echo dependence on pitch angle and flux minima at 90°, including increasing drift period toward 90° also evident in REPT observations. Dashed vertical line indicates impulse arrival at 0445UT at the magnetopause. Flux is normalized by the highest value in each energy bin, and color bar is scaled to show the gradient between 0.4% and 20% of the maximum value, similar to relative flux scaling in each energy bin of Figure 2.

5. Conclusions

The March 1991 shock injection event which produced new ultrarelativistic radiation belts (both electrons and protons) altered the static view of the radiation belts which preceded the CRRES measurements (Hudson et al., 2008). While the Halloween 2003 storm received comparable or greater attention (Baker et al., 2004), both events lacked key components which have been available during the Van Allen Probes era, when IP shock-induced geomagnetic storms have been more moderate: namely, simultaneous solar wind measurements and near-equatorial plane energetic particles and fields measurements.

The 17 March 2015 IP shock compression of the dayside magnetopause yields a well-measured example of the magnetosonic impulse injection mechanism responsible for the creation of a flux enhancement on less than a drift timescale, evident in multiple drift echoes indicative of prompt acceleration over a limited range of longitude. This event and the 7 October 2013 event reported by Foster et al. (2015) allow us to relax assumptions that were made in modeling the prior events. The magnitude of the electric field impulse ~ 10 mV/m on the dayside inferred from MHD simulations was comparable to that measured on the dayside for the 7 October 2013 event (Foster et al., 2015), and both were much smaller than that inferred from CRRES measurements on the nightside for the March 1991 event, extrapolated to ~ 200 mV/m on the dayside (Wygant et al., 1994) and inferred from MHD simulations for the Halloween 2003 event (Kress et al., 2007).

The difference in strength of E_Φ affects the radial transport of electrons inward (Gannon et al., 2005), which can be determined from the radial distance that an electron moves at a velocity $\sim E_\Phi/B$ over the time interval of the impulse interaction (Foster et al., 2015; Wygant et al., 1994). This δL is less than 1 for E_Φ ~10 mV/m starting at $L = 6.6$ over the energy range of Figure 2 and larger at higher L as **B** decreases, in contrast to the injection into $L = 2.5$ observed for the March 1991 event. With the ensuing inward motion of the magnetopause, the newly enhanced multi-MeV population is short lived, as evident in Figures 1 and 2 of Kanekal et al. (2016), in contrast to the two events with inferred E_Φ larger by an order of magnitude, March 1991 and Halloween 2003 storms. These produced flux enhancements observed by the low-altitude polar orbiting Solar Anomalous and Magnetospheric Particle Explorer (SAMPEX) spacecraft lasting for months to years (Looper et al., 2005).

The production of a multi-MeV enhancement at low $L \sim 2.5$ is resistant to magnetopause loss that was inferred for the 17 March 2015 event in pitch angle distribution measurements at higher L, as well as loss to the atmosphere due to whistler mode hiss trapped within the plasmapause which produces the slot region (Lyons et al., 1972). The latter has an increasingly long timescale at multi-MeV energies such that observations at SAMPEX for the Halloween 2003 event were delayed by months at low altitude due to the strongly peaked (at 90°) pitch angle distribution that resulted from radial transport (Looper et al., 2005). Acceleration by drift resonance with E_Φ increases perpendicular energy but not parallel, and thus the enhanced flux at 90° pitch angle (evident in drift echoes observed at lower $L \sim 3$ by Van Allen Probe A; see Kanekal et al. (2016)) must isotropize over the timescale of pitch angle diffusion, which is slow at high energies (Kress et al., 2007). Thus, the mechanism analyzed here is important for very strong IP shock events with drift echoes which produce rapid radial transport to a region and energy range where the new population is protected from rapid magnetopause and fast atmospheric losses, but less so for the two weaker IP shock events reported during the Van Allen Probes era. In the latter cases, the new population is short lived on the geomagnetic storm timescale. However, the mechanism proposed to explain the remarkable March 1991 injection holds up under these more modest conditions.

We have been able to reproduce for the first time using MHD test particle simulations the drift echoes that brought this mechanism to the attention of the radiation belt community with the CRRES observations. The drift-resonant acceleration mechanism remains a potential space weather threat because of the rapid timescale for flux enhancement, less than a multi-MeV electron drift period, and the persistence of such electrons once transported to low L values and sufficiently high energies.

Acknowledgments
This work was supported by JHU/APL under NASA contracts NNN16AA09T and NNN06AA01C to U. M. N. and U. N. H. with subcontracts to Dartmouth. We would like to acknowledge high-performance computing support from Yellowstone provided by NCAR's Computational and Information Systems Laboratory, supported by the National Science Foundation. Van Allen Probe ECT data can be accessed at https://www.rbsp-ect.lanl.gov/rbsp_ect.php and EFW survey plots at http://rbsp.space.umn.edu/survey/.

References

Ali, A. F., Malaspina, D. M., Elkington, S. R., Jaynes, A. N., Chan, A. A., Wygant, J., & Kletzing, C. A. (2016). Electric and magnetic radial diffusion coefficients using the Van Allen Probes data. *Journal of Geophysical Research: Space Physics*, *121*, 9586–9607. https://doi.org/10.1002/2016JA023002

Angelopoulos, V. (2011). The Artemis mission. *Space Science Reviews*, *165*(1–4), 3–25. https://doi.org/10.1007/ s11214-010-9687-2

Baker, D., Jaynes, A., Hoxie, V., Thorne, R., Foster, J., Li, X., … Lanzerotti, L. J. (2014). An impenetrable barrier to ultrarelativistic electrons in the Van Allen radiation belts. *Nature*, *515*(7528), 531–534. https://doi.org/10.1038/nature13956

Baker, D. N., Jaynes, A., Kanekal, S., Foster, J., Erickson, P., Fennell, J., … Wygant, J. R. (2016). Highly relativistic radiation belt electron acceleration, transport, and loss: Large solar storm events of March and June 2015. *Journal of Geophysical Research: Space Physics*, *121*, 6647–6660. https://doi.org/10.1002/2016JA022502

Baker, D., Kanekal, S., Li, X., Monk, S., Goldstein, J., & Burch, J. (2004). An extreme distortion of the Van Allen belt arising from the Halloween solar storm in 2003. *Nature*, *432*(7019), 878–881. https://doi.org/10.1038/nature03116

Blake, J., Kolasinski, W., Fillius, R., & Mullen, E. (1992). Injection of electrons and protons with energies of tens of MeV into l< 3 on 24 March 1991. *Geophysical Research Letters*, *19*(8), 821–824. https://doi.org/10.1029/92GL00624

Claudepierre, S., Mann, I., Takahashi, K., Fennell, J., Hudson, M., Blake, J., … Wygant, J. R. (2013). Van Allen Probes observation of localized drift resonance between poloidal mode ultra-low frequency waves and 60 keV electrons. *Geophysical Research Letters*, *40*, 4491–4497. https://doi.org/10.1002/grl.50901

Elkington, S. R., Hudson, M. K., & Chan, A. A. (2003). Resonant acceleration and diffusion of outer zone electrons in an asymmetric geomagnetic field. *Journal of Geophysical Research: Space Physics*, *108*, 1116. https://doi.org/10.1029/2001JA009202

Elkington, S. R., Hudson, M. K., Wiltberger, M. J., & Lyon, J. G. (2002). MHD/particle simulations of radiation belt dynamics. *Journal of Atmospheric and Solar-Terrestrial Physics*, *64*(5), 607–615. https://doi.org/10. 1016/S1364-6826(02)00018-4

Elkington, S. R., Wiltberger, M., Chan, A. A., & Baker, D. N. (2004). Physical models of the geospace radiation environment. *Journal of Atmospheric and Solar-Terrestrial Physics*, *66*(15), 1371–1387. https://doi.org/10.1016/j.jastp.2004.03.023

Foster, J., Wygant, J., Hudson, M., Boyd, A., Baker, D., Erickson, P., & Spence, H. E. (2015). Shock-induced prompt relativistic electron acceleration in the inner magnetosphere. *Journal of Geophysical Research: Space Physics*, *120*, 1661–1674. https://doi.org/10.1002/2014JA020642

Gannon, J., Li, X., & Temerin, M. (2005). Parametric study of shock-induced transport and energization of relativistic electrons in the magnetosphere. *Journal of Geophysical Research: Space Physics*, *110*, A12206. https://doi.org/10.1029/2004JA010679

Hudson, M. K., Baker, D., Goldstein, J., Kress, B., Paral, J., Toffoletto, F., & Wiltberger, M. (2014). Simulated magnetopause losses and Van Allen Probe flux dropouts. *Geophysical Research Letters*, *41*, 1113–1118. https://doi.org/10.1002/2014GL059222

Hudson, M., Brito, T., Elkington, S., Kress, B., Li, Z., & Wiltberger, M. (2012). Radiation belt 2D and 3D simulations for CIR-driven storms during Carrington Rotation 2068. *Journal of Atmospheric and Solar-Terrestrial Physics*, *83*, 51–62.

Hudson, M., Elkington, S., Lyon, J., Marchenko, V., Roth, I., Temerin, M., … Wygant, J. (1997). Simulations of radiation belt formation during storm sudden commencements. *Journal of Geophysical Research: Space Physics*, *102*(A7), 14,087–14,102.

Hudson, M., Kotelnikov, A., Li, X., Roth, I., Temerin, M., Wygant, J., … Gussenhoven, M. (1995). Simulation of proton radiation belt formation during the March 24, 1991 SSC. *Geophysical Research Letters*, *22*(3), 291–294.

Hudson, M. K., Kress, B. T., Mueller, H.-R., Zastrow, J. A., & Blake, J. B. (2008). Relationship of the Van Allen radiation belts to solar wind drivers. *Journal of Atmospheric and Solar-Terrestrial Physics*, *70*(5), 708–729. https://doi.org/10.1016/j.jastp.2007.11.003

Hudson, M., Paral, J., Kress, B., Wiltberger, M., Baker, D., Foster, J., … Wygant, J. (2015). Modeling CME-shock-driven storms in 2012–2013: MHD test particle simulations. *Journal of Geophysical Research: Space Physics*, *120*(2), 1168–1181. https://doi.org/10.1002/2014JA020833

Kanekal, S., Baker, D., Fennell, J., Jones, A., Schiller, Q., Richardson, I., … Wygant, J. R. (2016). Prompt acceleration of magnetospheric electrons to ultrarelativistic energies by the 17 March 2015 interplanetary shock. *Journal of Geophysical Research: Space Physics*, *121*, 7622–7635. https://doi.org/10.1002/2016JA022596

Kress, B., Hudson, M., Looper, M., Albert, J., Lyon, J., & Goodrich, C. (2007). Global MHD test particle simulations of > 10 MeV radiation belt electrons during storm sudden commencement. *Journal of Geophysical Research*, *112*, A09215. https://doi.org/10.1029/2006JA012218

Kress, B. T., Hudson, M. K., & Paral, J. (2014). Rebuilding of the Earth's outer electron belt during 8–10 October 2012. *Geophysical Research Letters*, *41*, 749–754. https://doi.org/10.1002/2013GL058588

Li, X., Baker, D., Temerin, M., Reeves, G., & Belian, R. (1998). Simulation of dispersionless injections and drift echoes of energetic electrons associated with substorms. *Geophysical Research Letters*, *25*(20), 3763–3766. https://doi.org/10.1029/1998GL900001

Li, Z., Hudson, M., Patel, M., Wiltberger, M., Boyd, A., & Turner, D. (2017). ULF wave analysis and radial diffusion calculation using a global MHD model for the 17 March 2013 and 2015 storms. *Journal of Geophysical Research*, *22*, 7353–7363. https://doi.org/10.1002/2016JA023846

Li, X., Roth, I., Temerin, M., Wygant, J., Hudson, M., & Blake, J. (1993). Simulation of the prompt energization and transport of radiation belt particles during the March 24, 1991 SSC. *Geophysical Research Letters*, *20*(22), 2423–2426. https://doi.org/10.1029/93GL02701

Looper, M., Blake, J., & Mewaldt, R. (2005). Response of the inner radiation belt to the violent Sun-Earth connection events of October–November 2003. *Geophysical Research Letters*, *32*, L03S06. https://doi.org/10.1029/2004GL021502

Lyon, J., Fedder, J., & Mobarry, C. (2004). The Lyon–Fedder–Mobarry (LFM) global MHD magnetospheric simulation code. *Journal of Atmospheric and Solar-Terrestrial Physics*, *66*(15), 1333–1350. https://doi.org/10.1016/j. jastp.2004.03.020

Lyons, L. R., Thorne, R. M., & Kennel, C. F. (1972). Pitch-angle diffusion of radiation belt electrons within the plasmasphere. *Journal of Geophysical Research*, *77*(19), 3455–3474. https://doi.org/10.1029/JA077i019p03455

Mauk, B., Fox, N. J., Kanekal, S., Kessel, R., Sibeck, D., & Ukhorskiy, A. (2013). Science objectives and rationale for the Radiation Belt Storm Probes mission. *Space Science Reviews*, *179*(1–4), 3–27. https://doi.org/10.1007/s11214-012-9908-y

Merkin, V., & Lyon, J. (2010). Effects of the low-latitude ionospheric boundary condition on the global magnetosphere. *Journal of Geophysical Research*, *115*, A10202. https://doi.org/10.1029/2010JA015461

Nishida, A. (1994). The Geotail mission. *Geophysical Research Letters*, *21*(25), 2871–2873. https://doi.org/10. 1029/94GL01223

Paral, J., Hudson, M., Kress, B., Wiltberger, M., Wygant, J., & Singer, H. (2015). Magnetohydrodynamic modeling of three Van Allen Probes storms in 2012 and 2013. *Annales Geophysicae*, *33*(8), 1037–1050.

Pembroke, A., Toffoletto, F., Sazykin, S., Wiltberger, M., Lyon, J., Merkin, V., & Schmitt, P. (2012). Initial results from a dynamic coupled magnetosphere-ionosphere-ring current model. *Journal of Geophysical Research: Space Physics*, *117*, A02211. https://doi.org/10.1029/2011JA016979

Roederer, J. G. (1970). *Dynamics of geomagnetically trapped radiation* (Vol. 2). Berlin, New York: Springer.

Shprits, Y., Thorne, R., Friedel, R., Reeves, G., Fennell, J., Baker, D., & Kanekal, S. (2006). Outward radial diffusion driven by losses at magnetopause. *Journal of Geophysical Research*, *111*, A11214. https://doi.org/10.1029/2006JA011657

Sibeck, D., McEntire, R., Lui, A., Lopez, R., & Krimigis, S. (1987). Magnetic field drift shell splitting: Cause of unusual dayside particle pitch angle distributions during storms and substorms. *Journal of Geophysical Research: Space Physics*, *92*(A12), 13,485–13,497.

Spence, H. E., Reeves, G., Baker, D., Blake, J., Bolton, M., Bourdarie, S., … Thorne, R. M. (2013). Science goals and overview of the Radiation Belt Storm Probes (RBSP) energetic particle, composition, and thermal plasma (ECT) suite on NASA Van Allen Probes mission. *Space Science Reviews*, *179*(1-4), 311–336. https://doi.org/10.1007/s11214-013-0007-5

Vampola, A. (1996). The ESA outer zone electron model update, *Environment Modeling for Space-Based Applications* (Vol. 392, pp. 151). Noordwijk, NL: European Space Agency.

Wygant, J., Bonnell, J., Goetz, K., Ergun, R., Mozer, F., Bale, S., … Tao, J. B. (2013). The electric field and waves instruments on the Radiation Belt Storm Probes mission. *Space Science Reviews*, *179*(1–4), 183–220. https://doi.org/201310.1007/s11214-013-0013-7

Wygant, J., Mozer, F., Temerin, M., Blake, J., Maynard, N., Singer, H., & Smiddy, M. (1994). Large amplitude electric and magnetic field signatures in the inner magnetosphere during injection of 15 MeV electron drift echoes. *Geophysical Research Letters*, *21*(16), 1739–1742. https://doi.org/10.1029/94GL00375